



Finite element analysis of friction stir welding process to predict temperature distribution

Vijayakumar Palanivel¹ , Pradeep Johnson², Arunkumar Munimathan^{2,4} ,
Sundaravadivel Thondamuthur Arumugam³

¹Nehru Institute of Technology, Department of Aeronautical Engineering, 641105, Coimbatore, India.

²Hindusthan College of Engineering and Technology, Department of Mechatronics Engineering, 641032, Coimbatore, India.

³R.M.D. Engineering College, Department of Mechanical Engineering, 601206, Chennai, India.

⁴University Centre for Research & Development, Department of Mechanical Engineering, Chandigarh University, Gharuan, Mohali, Punjab, India.

e-mail: thermalvijay@gmail.com, pradeepjohnson73@gmail.com, mrrarunapdpi@gmail.com, tas.snh@rmd.ac.in

ABSTRACT

Friction Stir Welding (FSW) is a solid-state joining technique which attained significant awareness due to its ability to produce high-quality welds without melting the base materials. The distribution of temperature across the plates during the FS Welding process is critical for determining the microstructural evolution, mechanical properties, and residual stresses of the welded joints. This research article aims to develop a comprehensive finite element (FE) model to predict the temperature distribution during the FS Welding process. The FE model incorporates the coupled thermo-mechanical behaviour of the FS Welding process, considering the heat generation and temperature-dependent material characteristics, plastic deformation and friction, and also the effect of tool geometry. The model is validated using experimental measurements, and the results obtained shows the simulated values representing the highest temperature obtained with respect to experimental values are within an error percentage of 3% from the experimental values and thereby validating the FEA procedure.

Keywords: Finite element (FE) model; Solid-state joining technique; Friction Stir Welding; Measurements; Mechanical behaviour.

1. INTRODUCTION

Friction Stir Welding, often known as FSW, is a cutting-edge solid-state joining process which garnered a lot of attention in a variety of sectors due to its capacity to generate welds of superior quality that have outstanding mechanical qualities [1–5]. During the procedure, a spinning tool that has a pin and shoulder is used to dive into the workpiece and move along the joining line. This causes friction and plastic deformation, which results in heat generation [6]. The technique can be successfully used to join various structural alloys such as Al-alloys in similar and dissimilar combinations, Mg-alloys, Cu-alloys, and steels [7–13]. FSW technique is utilized to achieve high-strength friction stir welded joints for large/extra-large thick plate structures, and also aluminium AA7075 and AA2024 alloys. Also this method is employed in nuclear power plants to weld neutron-irradiated 304L stainless steel. Friction stir lap welding was used to weld aluminum/steel dissimilar metals. Double-sided friction stir welding (SDS-FSW) technique was developed and investigated for welding 6 mm thick 6061 aluminum alloy joints. Further a study on how corrosion and mechanical characteristics of friction stir welded dissimilar 6101-T6 and 7075-T651 Aluminium Alloys were carried out to ascertain the effects of variable parameters such as the tool rotational and welding speeds. An electrically-magnetically-assisted friction stir welding (EMAFSW) method, conducting butt welding experiments on T76 tempered spray-formed 7055 aluminum alloy were carried out and compared to traditional friction stir welding (FSW) processes. Tool pin offset technique was employed to weld aluminum alloys AA 6013-T6 and AA 7075-T651 and mechanical and microstructural properties were investigated [14–21].

When it comes to defining the microstructural development, mechanical characteristics, and residual stresses of the welded joints, the temperature distribution that takes place throughout the FSW process is an extremely important factor [22]. Visualization and analysis of the material flow, temperature map, stresses and strains involved during the process is much easier in simulations than in experiments. The numerical modeling can provide mechanical and thermal histories of material particles, which are necessary to compute final

microstructure of the weld. Thus the numerical tool can also be helpful for understanding and controlling the final microstructure and properties of welds. Also simulations could help to adjust and optimize the process parameters and tool designs in order to achieve the best weld properties, increase welding rates and tool life, and enlarge the application field of the process by reducing stresses on FSW tool. The main purpose of this numerical simulation is to develop a 3D robust numerical tool enabling the thermo-mechanical simulation of the whole FSW process and also to find out the temperature distribution. This will help to predict the thermal stress that is induced during the FSW process. It has become clear that finite element modelling, sometimes known as FE modelling, is an effective method for forecasting the temperature distribution in FSW. In the beginning, finite element models were primarily concerned with heat transfer analysis, and they ignored material flow and deformation [22, 23]. In subsequent models, the coupled thermo-mechanical behaviour of the FSW process was added. This conduct took into account the heat production that happened due to plastic deformation along with friction, as well as temperature-dependent material characteristics and the impact of tool shape [24]. The integration of microstructural evolution and the prediction of mechanical characteristics have been the primary focuses of recent developments in finite element modelling of finite solid works (FSW) [25, 26]. Friction Stir Welding, often known as FSW, is a solid-state joining procedure that does not require the materials to be melted while the application is being performed [27]. The plastic deformation and friction brought on by the tool's rotational and transverse motions might cause the materials to become more pliable and stirred as a result of the heat that is created by these movements [28]. The absence of cracking and porosity, as well as the absence of any loss of alloying elements, are the defining characteristics of FSW joints [29]. The heat that is created due to FSW process as a result of friction and plastic deformation at the tool-workpiece interface, as well as the heat that is generated owing to plastic deformation in the thermo-mechanically impacted zone, causes the metal that is close to the tool to become significantly more pliable [30]. To fully comprehend the FS Welding process, it is essential to carry out a thermo mechanical study [31]. It is recommended that numerical simulation techniques, like finite element method (FEM), be utilized to carry out such a study [32]. To model the thermo-mechanical processes in FSW, the applications of computational fluid dynamics (CFD) and computational solid mechanics (CSM) methods were utilized [33]. In order to perform computational analysis, the mesh size needs to be comparable to or lower than 0.1 millimeters [34, 35]. The model's friction coefficient needs to be taken into consideration as a relation to the strain rate and temperature [36]. It is possible that the Coulomb friction model will lead to the achievement of an exact and remarkable accuracy in the temperature distribution predictions [37]. It is the sliding friction that occurs between the workpiece and tool that induces the heat to be produced [38].

Within and around the agitated zone, FSW causes a significant increase in temperature and a significant degree of plastic deformation. This causes the material to undergo complicated movement, as well as enormous shear pressures in the plastically deformed material, which in turn causes the material's temperature to rise to around 80 percent of its melting point. The term of frictional heat has been integrated into the equations that have developed, with the assumption that a steady uniform pressure exists between the component and tool. The temperature field that would be characterized by the analytical model developed is depicted in Figure 1. A model consists of three parameters: traverse speed of tool, rotational velocity ω , and loading force F . These parameters are defined by the model. Owing to the frictional contact that exists between the workpiece and the tool, temperature at the contact surface also increases. The occurrence of FSW typically takes place as the temperature reaches between 70 and 90 percent of the material melting temperature in weld line zone that is being welded. In the current study, the temperature that was achieved around the weld line area is inside the range that was divulged. On the other hand, the highest temperature that was obtained has a temperature which is lower than workpiece's melting temperature. Additionally, in order to achieve a more realistic simulation, a rotating and moving tool was utilized rather than a heat source that was actively moving. The tool pin was not taken into consideration. It is observed that the heat produced at the pin was little because it only accounted for around two percent of the overall heat. A tool that is constructed of a material that is tougher than the material of the workpiece that is being welded is often required for the FSW process. In the past, FSW processes were utilized for the processing of soft workpiece materials like aluminum. FSW has made it feasible to combine high-temperature materials like stainless steel. This change came about as a result of tool development's utilizing super-abrasive materials like polycrystalline cubic boron nitride (PCBN). It was tested that hard turning with varied edge design of PcBN inserts was successful. For simulation purpose, a cylindrical tungsten lanthanum oxide (W-1% La₂O₃) FSW tool model was utilized. For the purpose of simulating the clamping ends, workpiece edges parallel towards the weld line were given constraints in every direction. To imitate support at the bottom side of the workpiece, it was limited toward the direction that was perpendicular to the direction of the z-axis. Heat losses were taken into consideration over the entirety of the model's surfaces. When seen from the weld centerline, all of the boundary conditions were evenly distributed.

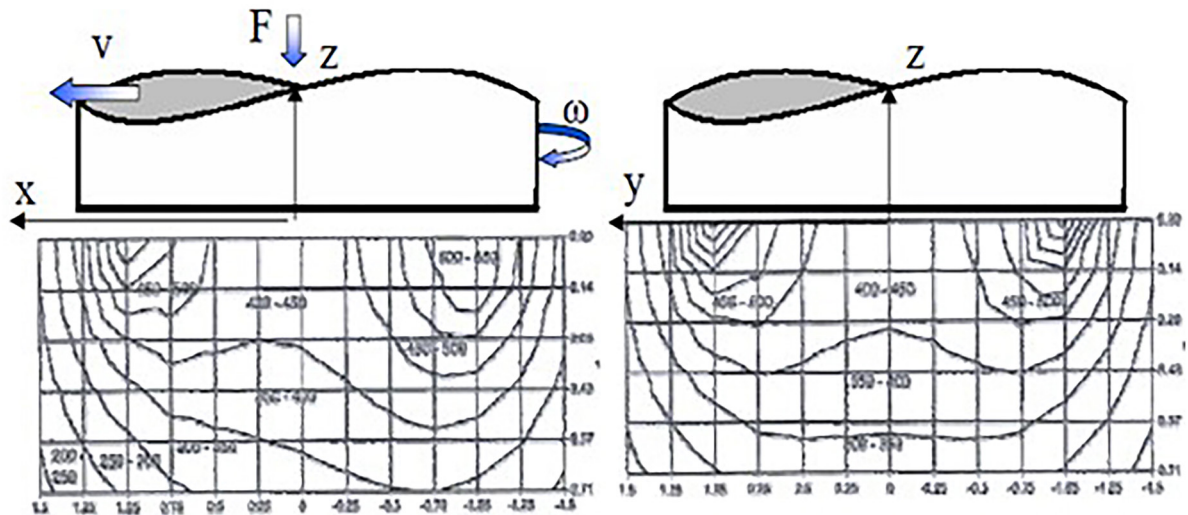


Figure 1: Longitudinal (leftside), Transverse (rightside) prints of temperature field calculated of analytical model of Gould and Feng (1998).

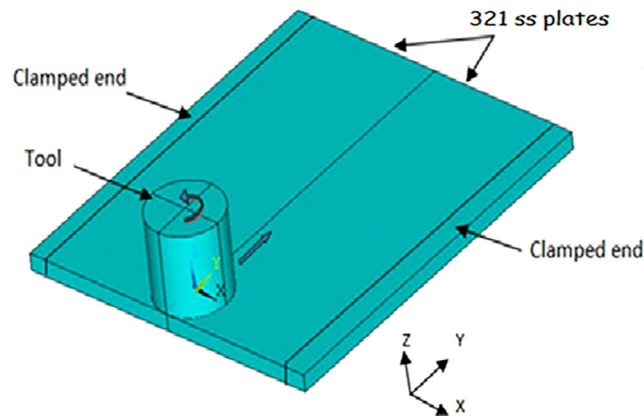


Figure 2: 3-D Model of workpiece and tool.

2. MATERIALS AND EXPERIMENTAL METHODS

2.1. Finite element model development

To forecast the dispensation of temperature in the welded components so as to replicate Friction Stir Welding (FSW) process, a three-dimensional finite element model was created. ANSYS Workbench 19.2, a multiphysics engineering simulation software was utilized to construct the model. The choice was made to employ the 'TRANSIENT THERMAL' analysis model to effectively simulate the transfer of heat phenomenon and reflect the time-dependent aspect of the welding process. The three-dimensional model takes into consideration the coupled thermo-mechanical behaviour during FSW process, taking into account the influence of tool shape, temperature-dependent material characteristics, and generation of during plastic deformation and friction. Figure 2 depicts solid model of two 321 stainless steel plates (workpiece) using a cylindrical-shaped tool.

2.2. Workpiece and tool modeling

Two plates with a rectangular form were employed as the workpiece. These plates were quite comparable to the ones that were used in the reference model. To cut down on the computational time, the dimensions were shrunk. $100 \times 50 \times 3 \text{ mm}^3$ was the dimensions of the plate. It had a shoulder diameter of twenty millimeters. The creation of heat and the increase in temperature in the region that was closest to the weld line were the primary focuses of discussion in this simulation. The coupled-field element SOLID226 was used to simulate the workpiece

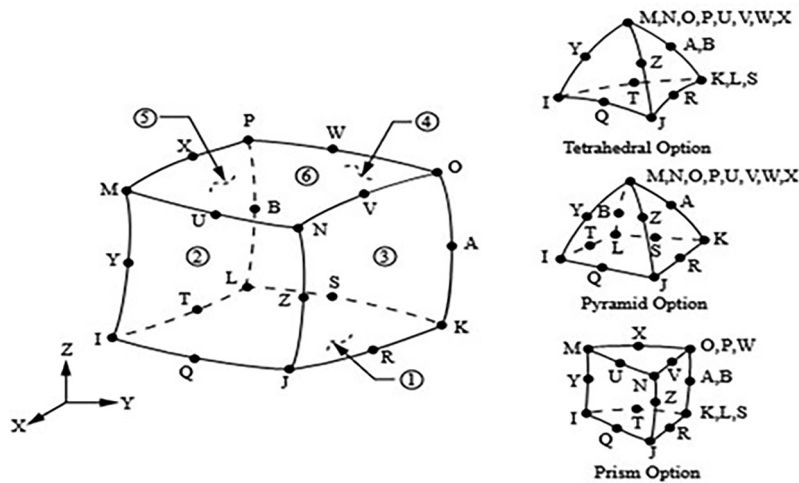


Figure 3: Geometry of element SOLID226.

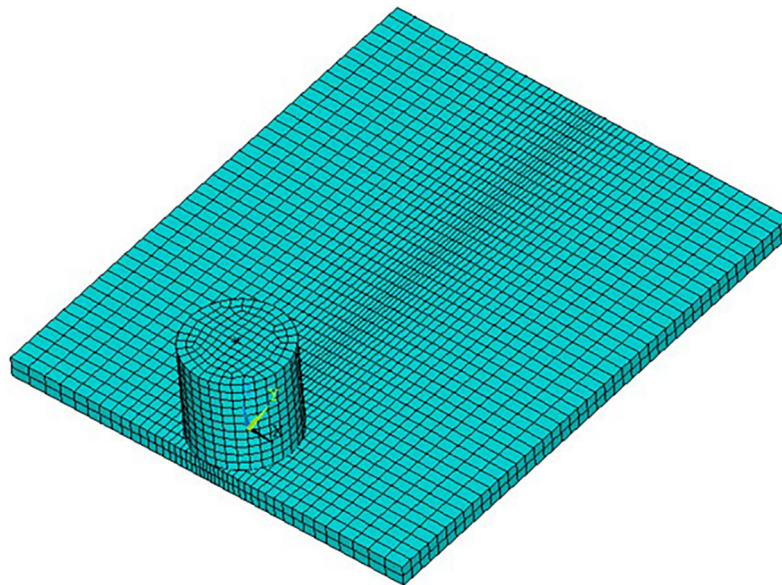


Figure 4: 3-D Meshed model of workpiece and tool.

(steel plates) and tool. The structural-thermal option was selected, and the KEYOPT(1) value was 11. There are twenty nodes comprised of the element, and each node can have up to six degrees of freedom. There are a number of structural capabilities, such as plasticity, elasticity, viscoelasticity, stress stiffening effects, viscoelasticity and deflection. For the purpose of conducting studies incorporating structural and thermal DOF (degrees of freedom), the thermoplastic and viscoelastic heating effects are provided. Figure 3 depicts the geometry of the SOLID226 system.

2.3. Mesh generation

It was necessary to build a tiny mesh with a size that was equivalent to or less than 0.1 mm in order to capture the steep temperature gradients and material flow patterns that were present in the welded zone. To correctly mimic the generation of heat and transmission, the mesh was improved in the regions that were close to the point where the tool and workpiece make contact. The tetrahedral mesh was replaced with a hexahedral mesh in order to alleviate the mesh-orientation dependency that was previously present. A more precise mesh was utilized in the weld-line region to obtain more precise outcomes. Figure 4 depicts the mesh model in three dimensions.

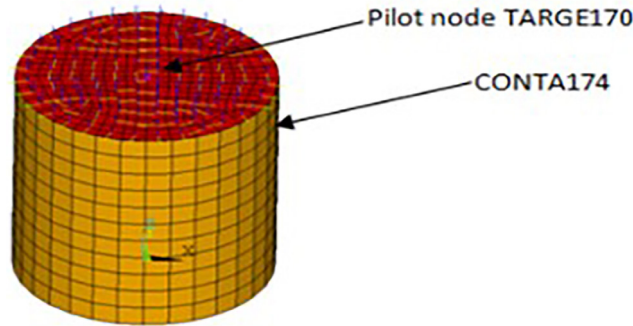


Figure 5: 3-D Rigid surface constrained.

Table 1: Material properties of workpiece.

Properties of 321 SS plates						
Young's Modulus	193 GPa					
Poisson's ratio	0.3					
Coefficient of Thermal Expansion	18.6 $\mu\text{m}/\text{m}^\circ\text{C}$					
(TB, BISO)						
Yield stress	205 MPa					
Tangent modulus	2.8 GPa					
Material properties relating to temperature						
Temperature ($^\circ\text{C}$)	0	200	400	600	800	1000
Thermal Conductivity ($\text{W}/\text{m}^\circ\text{C}$)	16	19	21	24	29	30
Specific Heat ($\text{J}/\text{Kg}^\circ\text{C}$)	500	540	560	590	600	610
Density (Kg/m^3)	8027	7894	7744	7631	7406	7406

2.4. Rigid surface constraint

Throughout the entirety of the simulation, the workpiece does not change anywhere. Along the weldline, the tool spins and advances in forward motion. It is necessary to establish a pilot node in the middle of the tool's upper surface in order to implement the tool's translation and rotation, as demonstrated in Figure 5. The movement of the pilot node determines the manner in which the complete tool moves. Between the tool's top surface nodes and the pilot node, a hard surface constraint is formed. This constraint is made between the two nodes.

2.5. Material properties

For the purpose of correctly capturing the thermo-mechanical behavior that occurs throughout the FSW process, the material characteristics of both the workpiece and the tool were characterized as being temperature-dependent. Due to the fact that the stresses and strains that are created during welding are reliant on temperature, it is exceptionally important that the FSW process has an accurate temperature estimate. There is a correlation between temperature and the thermal characteristics of the 321 steel plates, including specific heat, density and thermal conductivity. It is generally accepted that the mechanical characteristics of the stainless steel plates, like coefficient of thermal expansion, Young's modulus remain unchanged. Because of this, a bilinear isotropic hardening model, often known as TB, BISO is used. Table 1 presents the material parameters of the 321 stainless steel plates that are being discussed.

During the FSW process, approximately 80 percent of the plastic work is lost as heat at the end of the process. The Taylor–Quinney coefficient is a measure used in thermos mechanics that indicates the proportion of plastic work that is transformed into heat. After doing calculations to determine the effectiveness of the process, Taylor and Quinney came to the realization that around 90 percent of the plastic work was converted into heat. They discovered that a metal that had been plastically deformed was able to store a tiny percentage of plastic work, which resulted in an increase in the metal's internal energy. Therefore to determine the amount of plastic heat that is generated in the workpiece material, the Taylor-Quinney coefficient is fixed at 0.8. A tool made of a

Table 2: FSW tool material properties.

Young's Modulus	410 GPa
Poisson's ratio	0.3
Thermal Conductivity	120 W/m°C
Specific Heat	750 J/kg°C
Density	2581 kg/m ³

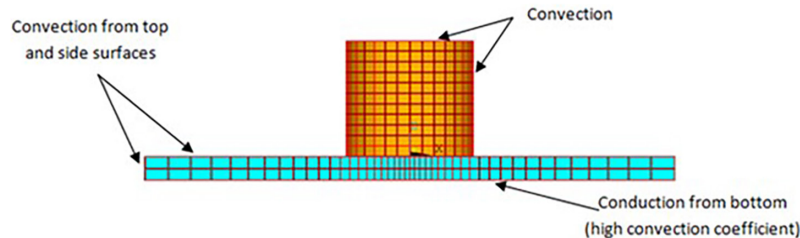


Figure 6: Thermal boundary conditions.

hard substance is necessary in order to successfully weld a material that is subjected to high temperatures, such as 321 stainless steel. The FSW tool that is utilized in this scenario is a cylindrical tungsten lanthanum oxide (W-1% La₂O₃) instrument. Table 2 depicts the tungsten lanthanum oxide (W-1% La₂O₃) FSW tool's material characteristics.

2.6. Loading and boundary conditions

The loading and boundary conditions were defined to simulate the actual FSW process. The rotational speed of tool, traverse speed, and axial force were applied as parameters for input data. The workpiece was fixed in place, and the tool was allowed to move along the joining line. The FSW model's mechanical and thermal boundary conditions are listed below.

- Thermal Boundary Conditions
- Mechanical Boundary Conditions
- Loading

2.7. Thermal boundary conditions

The frictional and thermal energy that is generated during FSW process is due to the plastic flow of material that quickly spreads towards remote parts of the plates. Radiation and Convection are the two mechanisms that are responsible for the heat loss to the surrounding environment on the workpiece's side and top surfaces [19]. Additionally, the workpiece's bottom surface is a potential source of conduction losses when it is connected to the backing plate. There is a representation of the thermal boundary conditions in Figure 6. It is determined that the convection coefficient of the workpiece and tool is 30 W/m²°C. It is estimated that heat loss due to conduction on the bottom surface of workpiece possesses a high heat transfer coefficient of 300 W/m²°C. This is significantly higher than the convective coefficient, which is approximately nine times higher. As a consequence of this, the workpiece's bottom surface is furthermore considered to be a convection surface when simulating conduction losses. Also the heat loss due to radiation is discarded because the percentage of heat that is lost as a result of radiation is very modest. A temperature of 25 degrees Celsius is used as the starting point for the model. Without exception, the model does not have any temperature boundary restrictions put on it.

2.8. Mechanical boundary conditions

While clamping each plate, the workpiece is secured in place. In every direction, the clamped sections of the plates are confined to their respective positions. It is necessary to limit all of the bottom nodes of the workpiece's orientation that is perpendicular towards the direction of plates in order to mimic support at the plate's base. Figure 7 illustrates the boundary conditions that are in place.

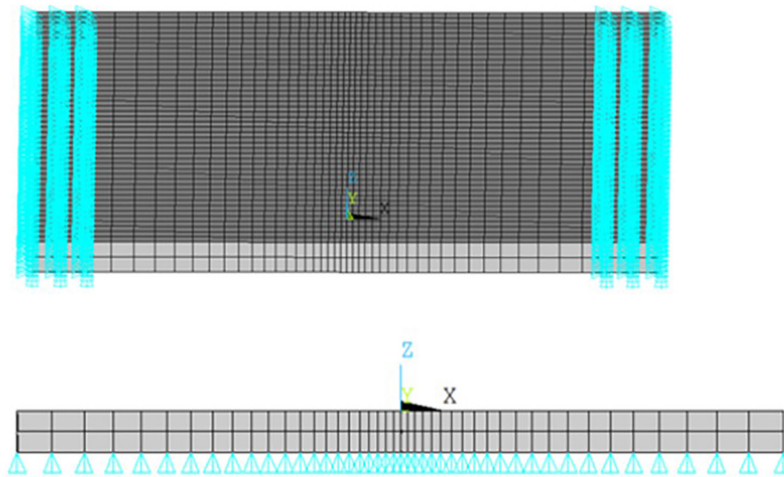


Figure 7: Meshed model with mechanical boundary conditions.

2.9. Numerical solution

For a speedier solution, automatic time-stepping was engaged. The beginning time stepsize (DELTIM) was fixed at 0.1. The minimal time step was fixed at 0.001. Maximum time step as 0.2 is employed in load steps 2 and 3, as an unconverged solution might arise due to larger maximum time-step size. An unconverged solution might arise from a larger maximum time-step size. The mesh or element size determines the time step values. The numerical solution was validated using experimental temperature measurements.

3. RESULTS AND DISCUSSIONS

The result of the investigation has provided an insight into forecasting the distribution of temperatures during friction stir welding process utilizing finite element analysis. This chapter provides a reflection of the research and its outcome, which were corroborated with the experimental results to validate the research.

3.1. Temperature distribution

The FE model that was constructed was used to make predictions about the distribution of temperatures that occurred during FSW procedure. According to the findings, the maximum temperature was found close to the point wherein the workpiece and tool make contact. This is the location where the least amount of heat was generated due to friction and plastic deformation. As one moved further from the tool, the temperature progressively reduced, which resulted in the formation of a temperature gradient within the welded zone. The following conclusions were reached utilizing the FSW simulation, which are presented below. A representation of the FSW simulation procedure depicted in Figure 8, which shows the temperature distribution following the third load stage.

3.2. Deformation

The occurrence of deflection in the workpiece due to the tool diving after the initial load step is depicted in Figure 9, which may be found below. Whenever an external load is applied to the stainless steel plate, it has a tendency to modify its position, its displacement, or its form. In the process of rigid body deformation, the plate does not change in size or shape from its initial state. It is also the case that the plate feels stress in this scenario since it is not just moving but rather absorbing part or all of the forces that are operating on it. Because of these forces, the body undergoes deformation, which is caused by the movement of particles, which in turn causes the body to change its shape.

3.3. Temperature results

Both Figures 10 and 11 illustrate the temperature distribution that occurs as a result of the origination of heat in the second and third load phases, respectively. During the last two load phases, the temperature of the workpiece achieves its highest point beneath the tool. The mechanical loads are the primary cause of this heat generation. No external heat sources were utilized. Increases in temperature cause the material to become more pliable, which results in a reduction in the coefficient of friction. The observed rise in temperature in the model, Figure 10 Temperature Distributions after Load Step 2 is illustrated in Figure 12, which demonstrates that the

NODAL SOLUTION
STEP=3
SUB =999999
TIME=29
TEMP (AVG)
DMX =.032262
SMN =25
SMX =1120.73

ANSYS
2019 R1
PLOT NO. 7

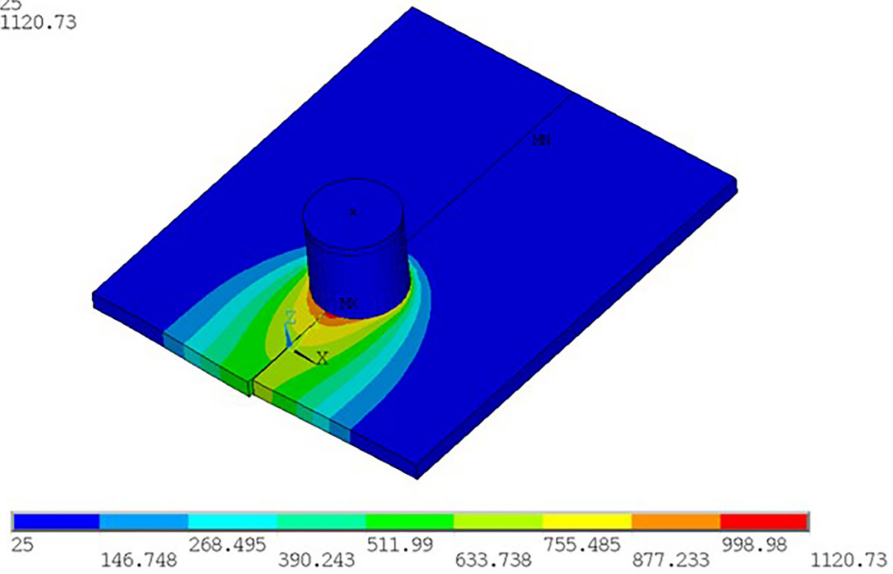


Figure 8: Temperature distributions in friction stir welded of 321 SS plates after the load step 3.

NODAL SOLUTION
STEP=1
SUB =10
TIME=1
UZ (AVG)
RSYS=0
DMX =.513E-06
SMN =-.303E-06
SMX =.215E-07

ANSYS
2019 R
PLOT NO. 1

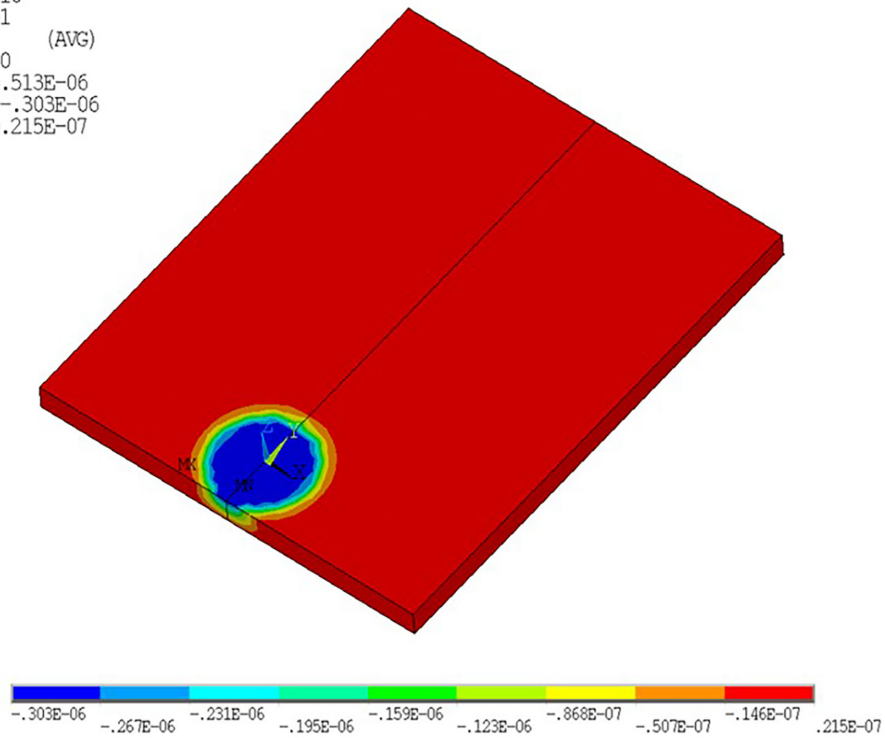


Figure 9: Deflection of workpiece after load step 1.

NODAL SOLUTION

STEP=2
SUB =205
TIME=6.5
TEMP (AVG)
DMX =.01525
SMN =24.9992
SMX =1016.48

ANSYS
2019 R1

PLOT NO. 6

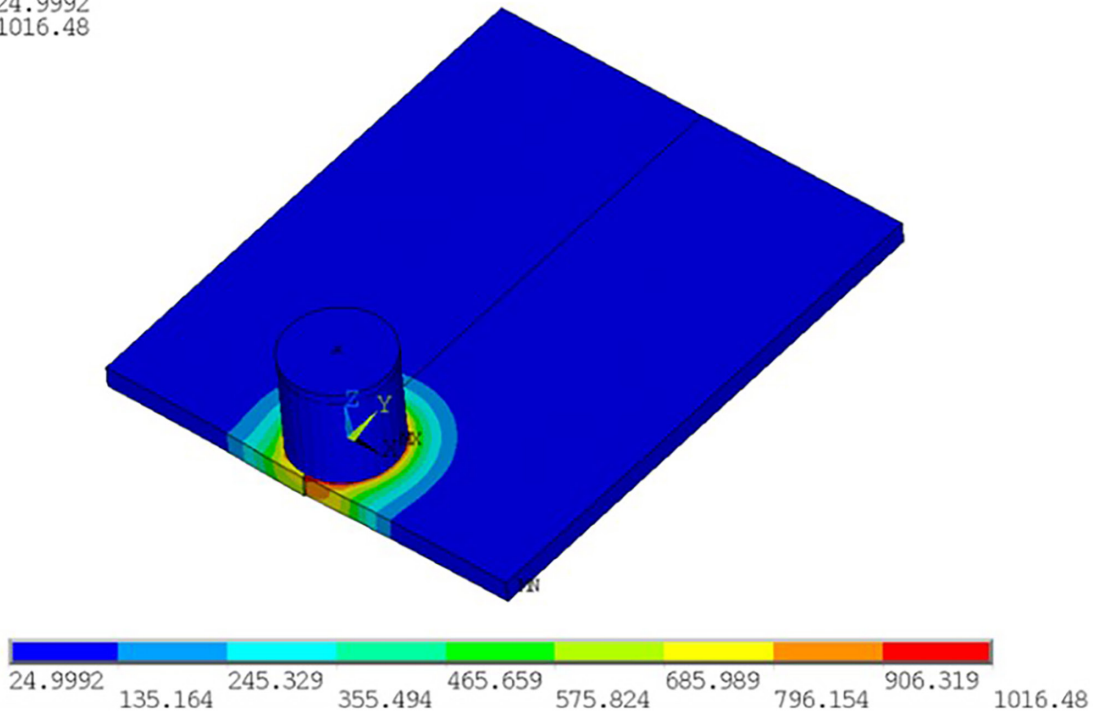


Figure 10: Temperature distribution after load step 2 (initial stage).

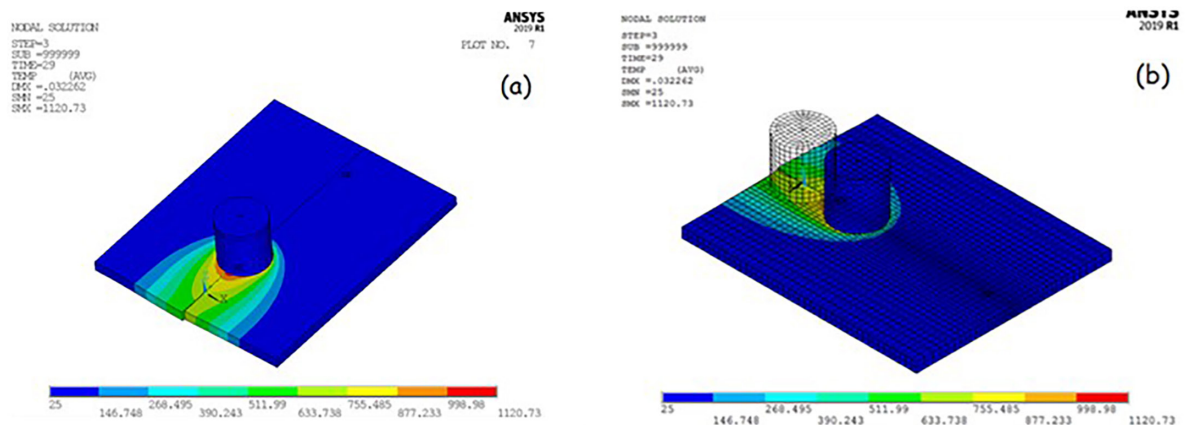


Figure 11: Temperature distribution after: (a) load step 2 and (b) load step 3.

development of heat occurs because of friction in second and third load among the tool shoulder and workpiece, and also the plastic deformation of the material that makes up the workpiece. Stainless steel with a 321 designation has a melting point that falls somewhere between 1400 and 1425 degrees Celsius. During the second and third load phases, the highest range of temperature occurs at weld line area on the workpiece under the tool area which is substantially lower than the workpiece's melting temperature. However, it is over 70% of the melting temperature. This is seen in the figure that follows. With temperatures falling within this range, the two plates are capable of being welded together. The usual time history plot that occurs throughout the FSW process is seen in Figure 13.

FCST26
max_temp

ANSYS
2019 R
PLOT NO. 1

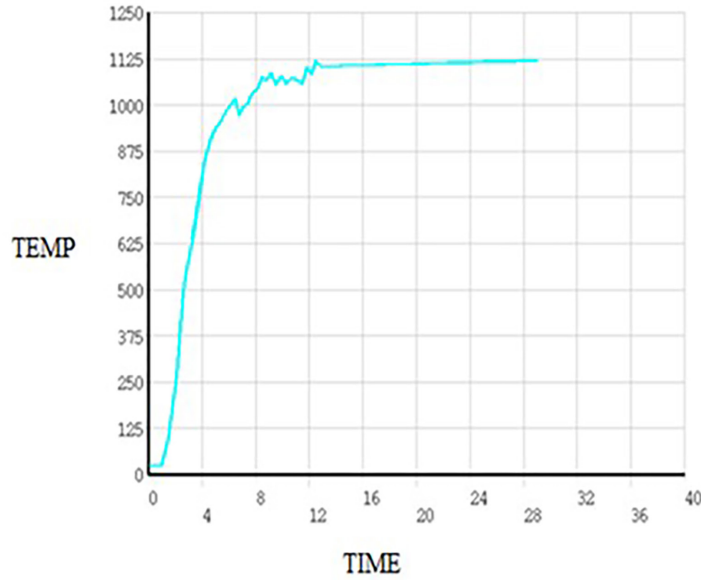


Figure 12: Typical time history plot of a point during FSW process.

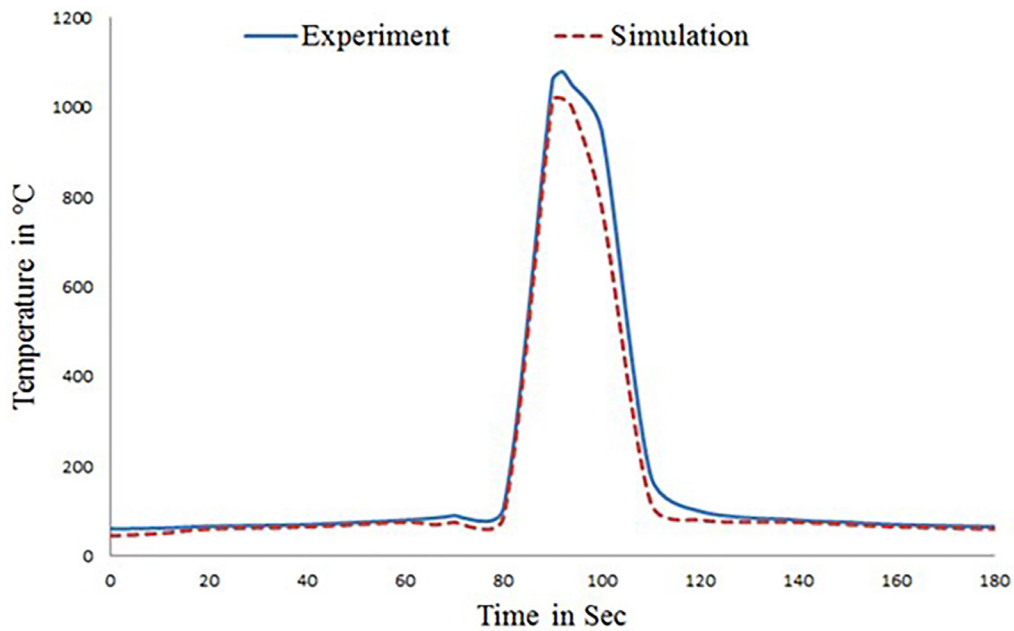


Figure 13: Time history plot of FSW of 321ss plates.

3.4. Validation with experimental data

For the purpose of validating the finite element model, experimental experiments was undertaken utilizing the use of the same welding settings and materials that were used in the simulations. Thermocouples were utilized in order to achieve temperature readings at a number of different sites along the weld line. To quantify the temperature distribution that occurred during the FS welding process, a thermocouple sensor of the K type was affixed to the oil-hardened backing steel plate. Silver paste was used to record the temperature that occurred while the

FS welding procedure was underway. An opening with a diameter of about 1.5 millimeters was drilled in the middle of the backing plate. This hole was designed in such a manner that the thermocouple bead would remain flat in the surface of the backing plate, just below the joint line.

An assessment of the finite element model's accuracy was undertaken by comparing the simulation results with the observations of the experimental temperature. The fact that the experimental and the numerical outcomes show strong correlation with each other demonstrates that the model that was constructed is valid.

The typical time history plot is depicted in Figure 13, and the time history plots that were produced from the FEA analysis are superimposed on the actual temperature graphs that are depicted in Figure 13 for the purpose of comparison and validation. As can be seen from the graphs, the anticipated temperatures are quite close to the actual temperatures, with just a little amount of fluctuation overall.

Figure 13 illustrate the maximum temperature that was determined by the finite element analysis (FEA) following the load stage. It is clear from the findings that the maximum temperature that was measured in the experiment and the maximum temperature that was anticipated are quite near to one another, and the percentage of mistake that was made in forecasting the maximum temperature was less than three percent.

4. CONCLUSIONS

Recently, finite element modelling has developed as a highly effective method for forecasting the temperature distribution in FSW environment. The finite element model that was built takes into consideration the coupled thermo-mechanical behaviour of the FSW process. This model takes into account the heat production that occurs as a result of friction and plastic deformation, as well as temperature-dependent material characteristics and the impact of machine geometry. Validation of the model was accomplished through the utilization of experimental measurements, and the outcomes offered valuable insights into the optimization of FSW process parameters in order to accomplish the appropriate temperature distributions. To corroborate the FEA approach that was followed in order to analyse the FSW process, it was discovered that the simulated values representing the highest temperature obtained with regard to experimental data revealed an error percentage that was within 3% of the experimental values. For the purpose of developing complete and dependable finite element models for finite surface wave (FSW), future research will concentrate on the integration of multi-physics phenomena, sophisticated material models, and efficient numerical approaches. It is possible to utilize the validated model to make predictions about the thermal behaviour of different material combinations and to provide support for the development of sophisticated FSW techniques for their use in industrial settings.

5. BIBLIOGRAPHY

- [1] MISHRA, R.S., MA, Z.Y., "Friction stir welding and processing", *Materials Science and Engineering R Reports*, v. 50, n. 1–2, pp. 1–78, 2005. doi: <http://doi.org/10.1016/j.mser.2005.07.001>.
- [2] AHMED, M.M.Z., EL-SAYED SELEMAN, M.M., FYDRYCH, D., *et al.*, "Friction stir welding in the aerospace industry: The current progress and state-of-the-art review", *Materials (Basel)*, v. 16, n. 8, pp. 2971, 2023. doi: <http://doi.org/10.3390/ma16082971>. PubMed PMID: 37109809.
- [3] CAM, G., IPEKOGLU, G., "Recent developments in joining of aluminium alloys", *International Journal of Advanced Manufacturing Technology*, v. 91, n. 5–8, pp. 1851–1866, 2017. doi: <http://doi.org/10.1007/s00170-016-9861-0>.
- [4] KASHAEV, N., VENTZKE, V., CAM, G., "Prospects of laser beam welding and friction stir welding processes for aluminum airframe structural applications", *Journal of Manufacturing Processes*, v. 36, pp. 571–600, 2018. doi: <http://doi.org/10.1016/j.jmapro.2018.10.005>.
- [5] CAM, G., "Friction stir welded structural materials: beyond Al-alloys", *International Materials Reviews*, v. 56, n. 1, pp. 1–48, 2011. doi: <http://doi.org/10.1179/095066010X12777205875750>.
- [6] COLEGROVE, P.A., SHERCLIFF, H.R., "3-Dimensional CFD modelling of flow round a threaded friction stir welding tool profile", *Journal of Materials Processing Technology*, v. 169, n. 2, pp. 320–327, 2005. doi: <http://doi.org/10.1016/j.jmatprotec.2005.03.015>.
- [7] TANG, Y., LI, W., ZOU, Y., *et al.*, "Effects of tool rotation direction on microstructure and mechanical properties of 6061 aluminum alloy joints by the synergistically double-sided friction stirwelding", *Journal of Manufacturing Processes*, v. 126, pp. 109–123, 2024. doi: <http://doi.org/10.1016/j.jmapro.2024.07.067>.
- [8] CAM, G., JAVAHERI, V., HEIDARZADEH, A., "Advances in FSW and FSSW of dissimilar Al-alloy plates", *Journal of Adhesion Science and Technology*, v. 37, n. 2, pp. 162–194, 2023. doi: <http://doi.org/10.1080/01694243.2022.2028073>.

- [9] AHMED, M.M.Z., EL-SAYED SELEMAN, M.M., FYDRYCH, D., *et al.*, “A review on friction stir welding of dissimilar Al- and Mg-alloys: scientometric analysis and strategies for achieving high-quality joints”, *J Magnes Alloy*, v. 11, n. 11, pp. 4082–4127, 2023. doi: <http://doi.org/10.1016/j.jma.2023.09.039>.
- [10] KHALIQ, U.A., YUSOF, F., *et al.*, “A comprehensive review on friction stir welding of aluminum with magnesium: A new insight on joining mechanisms by interfacial enhancement”, *Journal of Materials Research and Technology*, v. 27, pp. 4595–4624, 2023. doi: <http://doi.org/10.1016/j.jmrt.2023.10.158>.
- [11] KÜÇÜKÖMEROĞLU, T.E.V.F.İ.K., ŞENTÜRK, E., KARA, L., *et al.*, “Microstructural and mechanical properties of friction stir welded nickel-aluminum bronze (NAB) alloy”, *Journal of Materials Engineering and Performance*, v. 25, n. 1, pp. 320–326, 2016. doi: <http://doi.org/10.1007/s11665-015-1838-x>.
- [12] KUCUKOMEROGLU, T., AKTARER, S.M., IPEKOGLU, G., *et al.*, “Investigation of mechanical and microstructural properties of friction stir welded dual phase (DP) steel”, In: *IOP Conf Ser Mater Sci Eng*, 629, 012010, 2019.
- [13] IPEKOGLU, G., KUCUKOMEROGLU, T., AKTARER, S.M., *et al.*, “Investigation of microstructure and mechanical properties of friction stir welded dissimilar St37/St52 joints”, *Materials Research Express*, v. 6, n. 4, pp. 046537, 2019. doi: <http://doi.org/10.1088/2053-1591/aafb9f>.
- [14] XUE, W., SONG, N., LI, J., *et al.*, “Improving mechanical properties of 18 mm thick plate friction stir welding joint by combining the thermomechanical-fluid coupled model and partial least squares regression algorithm”, *Journal of Manufacturing Processes*, v. 126, pp. 443–470, 2024. doi: <http://doi.org/10.1016/j.jmapro.2024.07.069>.
- [15] RATHINASURIYAN, C., PUVIYARASAN, M., SANKAR, R., *et al.*, “Effect of process parameters on weld geometry and mechanical properties in friction stir welding of AA2024 and AA7075 alloys”, *Journal of Alloys and Metallurgical Systems*, v. 7, pp. 100091, 2024. doi: <http://doi.org/10.1016/j.jalms.2024.100091>.
- [16] GUSSEV, M.N., TANG, W., CHEN, X., *et al.*, “Microstructure and mechanical properties of friction stir weld performed on neutron-irradiated 304L steel with helium”, *Materials Characterization*, v. 209, pp. 113697, 2024. doi: <http://doi.org/10.1016/j.matchar.2024.113697>.
- [17] LIU, T., GAO, S., SHI, L., *et al.*, “Welding load, temperature, and material flow in ultrasonic vibration enhanced friction stir lap welding of aluminum alloy to steel”, *Materials Today. Communications*, v. 40, pp. 109894, 2024. doi: <http://doi.org/10.1016/j.mtcomm.2024.109894>.
- [18] TANG, Y., LI, W., ZOU, Y., *et al.*, “Effects of tool rotation direction on microstructure and mechanical properties of 6061 aluminum alloy joints by the synergistically double-sided friction stir welding”, *Journal of Manufacturing Processes*, v. 126, pp. 109–123, 2024. doi: <http://doi.org/10.1016/j.jmapro.2024.07.067>.
- [19] ABOLUSORO, O.P., KHOATHANE, M.C., MHIKE, W., *et al.*, “Influence of welding parameters and post weld heat treatment on mechanical, microstructures and corrosion behaviour of friction stir welded aluminium alloys”, *Journal of Materials Research and Technology*, v. 32, pp. 634–648, 2024. doi: <http://doi.org/10.1016/j.jmrt.2024.07.175>.
- [20] CHEN, X., CHEN, S., DUAN, R., *et al.*, “Study on the microstructure and properties of spray formed 7055-T76 aluminum alloy joints by rotating magnetic field assisted friction stir welding”, *Materials Characterization*, v. 214, pp. 114080, 2024. doi: <http://doi.org/10.1016/j.matchar.2024.114080>.
- [21] KASMAN, S., “The effects of pin offset for FSW of dissimilar materials: a study for AA 7075-AA 6013”, *Matéria (Rio de Janeiro)*, v. 25, n. 2, pp. e12612, 2020. doi: <http://doi.org/10.1590/s1517-707620200002.1012>.
- [22] CHAO, Y.J., QI, X., “Thermal and thermo-mechanical modeling of friction stir welding of aluminum alloy 6061-T6”, *Journal of Materials Processing Technology*, v. 146, n. 2, pp. 263–272, 1998.
- [23] FRIGAARD, Ø., GRONG, Ø., MIDLING, O.T., “A process model for friction stir welding of age hardening aluminum alloys”, *Metallurgical and Materials Transactions. A, Physical Metallurgy and Materials Science*, v. 32, n. 5, pp. 1189–1200, 2001. doi: <http://doi.org/10.1007/s11661-001-0128-4>.
- [24] DENG, X., XU, S., LUO, Y., “A three-dimensional numerical model for friction stir welding of aluminum alloys”, *Proceedings of the Institution of Mechanical Engineers. Part B, Journal of Engineering Manufacture*, v. 215, n. 11, pp. 1639–1649, 2001.
- [25] FEHRENBACHER, A., SCHMALE, J.R., ZINN, M.R., *et al.*, “Measurement of tool-workpiece interface temperature distribution in friction stir welding”, *Journal of Manufacturing Science and Engineering*, v. 136, n. 2, pp. 021009, 2014. doi: <http://doi.org/10.1115/1.4026115>.

- [26] CHIUMENTI, M., CERVERA, M., AGELET DE SARACIBAR, C., *et al.*, “Numerical modeling of friction stir welding processes”, *Computer Methods in Applied Mechanics and Engineering*, v. 254, pp. 353–369, 2007. doi: <http://doi.org/10.1016/j.cma.2012.09.013>.
- [27] MEYGHANI, B., WU, C., “Progress in thermomechanical analysis of friction stir welding”, *Chinese Journal of Mechanical Engineering*, v. 33, n. 12, pp. 12, 2020. doi: <http://doi.org/10.1186/s10033-020-0434-7>.
- [28] KHANDKAR, M.Z.H., KHAN, J.A., REYNOLDS, A.P., “Prediction of temperature distribution and thermal history during friction stir welding: input torque based model”, *Science and Technology of Welding and Joining*, v. 11, n. 2, pp. 165–174, 2006.
- [29] SALUJA, R.S., GANESH, K.V., “Multi-physics modeling of friction stir welding process: a review”, *Journal of Materials Processing Technology*, v. 229, pp. 179–202, 2016.
- [30] SCHMIDT, H., HATTEL, J., “A local model for the thermomechanical conditions in friction stir welding”, *Modelling and Simulation in Materials Science and Engineering*, v. 13, n. 1, pp. 77–93, 2005. doi: <http://doi.org/10.1088/0965-0393/13/1/006>.
- [31] SERIO, L.M., PALUMBO, D., DE FILIPPIS, L.A.C., *et al.*, “Effect of friction stir process parameters on the mechanical and thermal behavior of 5754-H111 aluminum plates”, *Materials (Basel)*, v. 9, n. 3, pp. 122, 2016. doi: <http://doi.org/10.3390/ma9030122>. PubMed PMID: 28773246.
- [32] ZHANG, H.W., ZHANG, Z., CHEN, J.T., “3D modeling of material flow in friction stir welding under different process parameters”, *Journal of Materials Processing Technology*, v. 183, n. 1, pp. 62–70, 2007. doi: <http://doi.org/10.1016/j.jmatprotec.2006.09.027>.
- [33] ASSIDI, M., FOURMENT, L., GUERDOUX, S., *et al.*, “Friction model for friction stir welding process simulation: Calibrations from welding experiments”, *International Journal of Machine Tools & Manufacture*, v. 50, n. 2, pp. 143–155, 2010. doi: <http://doi.org/10.1016/j.ijmachtools.2009.11.008>.
- [34] GOULD, J.E., FENG, Z., “Heat flow model for friction stir welding of aluminum alloys”, *Journal of Materials Processing & Manufacturing Science*, v. 7, n. 2, pp. 185–194, 1998. doi: <http://doi.org/10.1106/648R-2CNE-2PD0-45L6>.
- [35] PRASANNA, P., RAO, B.S., RAO, G.K.M., “Finite element modeling for maximum temperature in friction stir welding and its validation”, *International Journal of Advanced Manufacturing Technology*, v. 51, n. 9–12, pp. 925–933, 2010. doi: <http://doi.org/10.1007/s00170-010-2693-4>.
- [36] ZHU, X.K., CHAO, Y.J., “Numerical simulation of transient temperature and residual stresses in friction stir welding of 304L stainless steel”, *Journal of Materials Processing Technology*, v. 146, n. 2, pp. 263–272, 2004. doi: <http://doi.org/10.1016/j.jmatprotec.2003.10.025>.
- [37] ÖZEL, T., KARPAT, Y., SRIVASTAVA, A., “Hard turning with variable micro-geometry PcBN tools”, *CIRP Annals*, v. 57, n. 1, pp. 73–76, 2008. doi: <http://doi.org/10.1016/j.cirp.2008.03.063>.
- [38] SUBRAMANI, S., MUNIMATHAN, A., MANIVANNAN, J.M., *et al.*, “Mechanical properties: lifespan and retention forecast for jute fiber woven fabric reinforced epoxy matrix composite”, *Polymer Composites*, v. 45, n. 11, pp. 1–16, 2024. doi: <http://doi.org/10.1002/pc.28456>.